Received: 20 July 2020 | Revised: 12 October 2020 | Accepted: 20 October 2020

DOI: 10.1002/ces2.10074

ORIGINAL ARTICLE

International Journal of Ceramic Engineering & Science

The mineralogy of air granulated converter slag

Katrin Schollbach[1,2] | **Muhammad J. Ahmed**[1] | **Sieger R. van der Laan**[1,2]

[1]Department of the Built Environment, Eindhoven University of Technology, Eindhoven, The Netherlands

[2]Tata Steel, R&D, Microstructure & Surface Characterization (MSC), IJmuiden, The Netherlands

Correspondence
Katrin Schollbach, Department of the Built Environment, Eindhoven University of Technology, P. O. Box 513, 5600MB, Eindhoven, The Netherlands
Email: k.schollbach@tue.nl

Funding information
Tata Steel

Abstract

Converter slag, also known as Basic Oxygen Furnace slag, is a by-product of steelmaking that is produced in large quantities worldwide. It currently has few applications, because the presence of free lime often prevents the use as aggregate, while the low reactivity makes it undesirable as a cement replacement. Air granulation is a promising way to increase the reactivity of converter slag and enable recycling as a cement replacement and this is the first in-depth characterization of air granulated steel slag. In this study converter slag was separated into different fractions (0.25-0.5 mm, 0.5-1 mm, 1-2 mm, 2-4 mm) after air granulation to study the influence of size and therefore cooling speed on its mineralogy. The air granulated slag fractions were characterized using X-ray fluorescence, quantitative X-Ray diffraction, large area phase mapping based on scanning electron microscopy and energy-dispersive X-ray spectroscopy as well as leaching behavior. The results show that the main minerals in air granulated converter slag are the same as in industrially cooled slag, but that additional perovskite was formed, which has not been reported before. All fractions contained large phenocrysts of Ca_2SiO_4 and Mg-wuestite surrounded by a dense matrix containing the other minerals. The three largest fractions are very similar to each other in chemical composition and microstructure, while the smallest fraction (0.25-0.5 mm) contains a higher content of Mg-wuestite even though the starting composition was the same. Free lime is only present at the detection limit (0.1 ± 0.1 wt%) in all size fractions. The leaching of chromium and vanadium is greatly increased compared to standard cooled converter slag indicating that air granulation results in the greater dissolution of phases containing these elements, which also indicates a greater hydraulic reactivity of granulated slag despite very little amorphous content.

KEYWORDS
air granulation, converter steel slag, mineralogy

1 | INTRODUCTION

Converter slag is produced during the conversion of pig iron into steel in a basic oxygen furnace. For this reason, it is also called BOF-Slag or LD-slag after the Linz-Donawitz process.[1,2] On average 126 kg converter slag is produced per ton of steel,[3] with worldwide steel production of 1.8 Mt in 2019.[4] The oxide composition is variable, but converter slag tends to be very rich in CaO and Fe_2O_3 (30-50 wt%), with lower amounts of SiO_2 and MgO (10 to 20 wt%).[2,5]

Components such as MnO, Al_2O_3, P_2O_5, TiO_2 are present as minor oxides (2-5 wt%). Depending on the iron ore used, the slag can contain V_2O_5 and Cr_2O_3.[6,7] The main mineral phases in cement chemistry notation are α'_H-C_2S (α'_H-Ca_2SiO_4), β-C_2S (β-Ca_2SiO_4), (Fe,Mg)O and $C_2(A,F)$ ($Ca_2(Al,Fe)_2O_5$).[8] Additionally, magnetite (Fe_3O_4), C_3S (Ca_3SiO_5), free lime (CaO), and magnesia (MgO) can be present. Merwinite ($Ca_3Mg(SiO_4)_2$) has also been reported.[9,10]

The reuse of converter steel slag as a secondary raw material has been a challenge, and no economically successful applications have been developed so far. European statistical data from 2016[11] shows that more than 20% of the annual converter steel slag production has no use (intermediate storage or landfilled), while 46% has a low-added value application as road base material. Because it is available in large quantities and contains mineral phases also present in Portland cement, converter slag has been tested as a building material[12,13,14] However, the presence of free lime (CaO) and the volume expansion associated with its delayed hydration often prevent this type of application.[15] Milling converter slag to cement fineness, thereby exposing the free lime for hydration could solve the expansion problem. This may open up the use as a supplementary cementitious material and some promising results regarding the development of long-term strength in mortars have been reported.[16] However, the overall low reactivity of converter slag compared with Portland cement has hindered its widespread use as supplementary cementitious material.[17] Because of steel slags high strength and abrasion resistance, it has found some use as aggregate in asphalt.[18,19,20] Other suggested uses include the production of fertilizer,[21] the production of building materials via carbonation,[22] or the recovery of vanadium via leaching.[23] However, the first two applications are only suitable for converter slag that contains no or very little vanadium and chromium due to concerns about leaching,[24] while vanadium recovery is only feasible for slags containing sufficient vanadium.

However, the goals set by the Netherlands to reduce the use of raw materials 50% by 2030 and to have a completely waste-free, circular economy by 2050 means that applications have to be found.[25] Similar goals exist in the European Union as a whole.[26]

One strategy to make converter slag more reactive and realize an application in cement is fast cooling through granulation to prevent crystallization.[27] This technique is already used to produce amorphous blast furnace slag that has excellent properties as a pozzolanic material in Portland cement.[28] Air granulation specifically is also a promising way to recover heat from converter slag that has a temperature between 1,250 and 1,700°C when it is removed from the converter.[29] It could also help to stabilize C_3S, which is more reactive than C_2S.[30] The current industrial practice is to pour the liquid slag into pits and cool it using water. But the bulk of the slag still cools very slowly using this method (up to 24 hours), and the resulting slag is reported to be almost completely crystalline.[6,31]

A few studies have investigated the influence of cooling speed on converter slag mineralogy using different approaches. For example, Choi and Jung[31] re-melted converter slag under an argon atmosphere and then cooled it at speeds between 10-50°C/min starting from temperatures between 1,600 and 1,110°C. They concluded that these conditions did not generate significant amounts of amorphous phase because the slag crystallizes very rapidly. Gautier et al.[9] compared water granulated, industrially cooled, and intentionally slow cooled converter slag with each other. Their X-ray diffractograms were not quantified but do not show a significant decrease of the crystalline phase in the water granulated slag. They found, however, that slow cooling promoted the formation of C_2S and MgO, while fast cooling resulted in the formation of C_3S that later converted to free lime and C_2S. The cooling speed also significantly influenced the crystallite size of the phases. The connection between cooling speed and leaching properties was investigated by Tossavainen et al.[32], who compared water granulated and air-cooled with industrially produced converter slag. The results show a clear decrease in Ca, Fe, and Si leaching with increasing cooling speed. The reason for this is unclear and may be caused by mineralogical changes upon rapid cooling or surface area differences, as granulated slag tends to have a much lower surface area than irregularly broken, industrially cooled slag. Overall, the literature is limited and to the best of the authors' knowledge there is no information available about air granulated converter slag and a quantitative investigation of the influence of fast cooling on converter slag mineralogy is still missing.

This study investigates air granulated converter slag sieved into different size fractions (2-4 mm, 1-2 mm, 0.5-1 mm, 0.25-0.5 mm) to gain information about the influence of the cooling speed. The chemical bulk composition was measured with XRF, while the mineralogical composition was determined using quantitative XRD. SEM/EDX-based large area phase mapping using PARC (PhAse Recognition and Characterization) software was employed to determine microstructure, phase amounts, and average compositions. Leaching tests were carried out to determine the environmental impact and reactivity of the granulated slag. The results for the different slag sizes were compared with each other to gain insight into the state of converter slag before granulation, its crystallization behavior, and the influence of the cooling speed, which forms the basis for understanding converter slag reactivity. In turn, this could enable the recycling of large amounts of converter slag as a cement replacement material and reduce the CO_2 emissions of the building materials industry.

2 | MATERIALS AND METHODS

2.1 | Material

Converter slag taken from regular production at Tata Steel Europe in IJmuiden was granulated at Harsco Metals Holland B.V. in a make-shift experimental facility by pouring it in front of a strong air fan. The tap-temperature of the slag at the converter was 1592°C and the batch size 40 tons. A temperature drop of approximately 40°C is known to occur at tapping. Negligible further cooling of the slag takes place during transportation to the slag yard since it develops a self-insulating freeze lining against the slag pot (Tata proprietary reports). The slag temperature at granulation can, therefore, be expected to have been around 1,550°C, and 36 tons of slag were granulated while 4 tons of freeze-on slag remained in the slag pot. The exact cooling rate during granulation is unknown but depends on granule size. Larger slag granules cool slower than smaller ones. For this reason, the granulated slag was sieved in the laboratory and divided into the following size fractions: >4 mm (3.8 wt%), 2-4 mm (47.2 wt%), 1-2 mm (39 wt%), 0.5-1 mm (6.5 wt%), 0.25-5 mm (0.7 wt%) and < 0.25 mm (2.8 wt%). The fraction > 4 mm consisted of welded smaller granules and was not investigated further. The fraction < 0.25 mm was also excluded from further analysis, due to XRD measurements showing very high amounts of contamination that were likely introduced while collecting the granules from the slag yard. Fraction 0.25-5 mm also contained some contaminants such as blast furnace slag. Their influence on the analysis is discussed in the results. The complete mineralogical composition of all fractions is given in Table A1 in Appendix 1.

2.2 | Methods

Prior to analysis, the sieved granulated converter slag was dried at 100°C in a drying oven to remove any moisture that could react with the sample during grinding. No phase changes are expected at this temperature. Before XRF analysis the samples were heated to 1,000°C for 2 hours and the weight change recorded. The residue was then mixed with borate flux to make fused beads. To prepare the samples for XRD measurements, the granulated slag fractions were first ground in a disk mill, mixed with 10 wt% Si as an internal standard,[33] and then ground again in a Retsch McCrone XRD mill to a size of around 15 μm. The diffractograms were measured using a Bruker D8 with a Cu anode ($K\alpha_1$ 1.5406 Å, $K\alpha_2$ 1.5445 Å, energy filtering and a LynxEye detector. A 0.5° fixed divergence slit was used with a primary and secondary collimator of 2.5°. The phases in the diffractograms were identified using HighScore Plus 4.6a (PANalytical) and the PDF 2 database. Rietveld quantification was done with Topas 5 (Bruker).[34]

The sieved slag granules were embedded in resin (Struers EpoFix), cut, polished using alcohol-based diamond suspensions, and then coated with carbon before acquiring spectral imaging (SI) data sets for large area phase mapping. A JEOL JSM-7001F SEM equipped with two 30 mm^2 SDD detectors (Thermo Fisher Scientific) and NORAN-System7 hardware with NSS.3.3 software was used, with an accelerating voltage of 15 kV and a beam current of 6.2 nA. One SI field consisted of a data set of 512x384 data points, with a data point size of 1 μm. In order to get representative data set, several SI fields were measured and their total area was 30.2 (2-4 mm), 16.7 (1-2 mm), 17.8 (0.5-1mm), and 9.7 mm^2 (0.25-0.5 mm). The SI image sets were analyzed and stitched together using PhAse Recognition and Characterization (PARC) software developed by Tata steel.[6,35] PARC groups SI data points according to their composition determined with EDX and generates a phase map, phase amounts in area%, as well as the average composition of these phases. The chemical composition given here is the average of all SI fields analyzed, the error is the standard deviation between fields. To determine the size of the phenocrysts (C_2S and Mg-wuestite) in the air granulated converter slag phase maps, ImageJ[36] was used. Areas smaller than 10 μm^2 were removed from further evaluation to avoid artifacts that can occur because the resolution of the EDX is only about 1 μm^2 and does not return accurate values for very small grains. The grains were then sorted into size bins, normalized by the total area of the converter slag granules measured for each size fraction and recalculated to an equivalent diameter assuming a spherical shape for each grain. No stereological correction was applied to the data.

To eliminate some of the contamination of the granulated slag surface, dust was removed by washing with anhydrous isopropanol followed by diethyl ether. To eliminate all organic solvent, the sample was then dried in an oven at 40°C under vacuum. These samples were used to carry out a one batch leaching test according to NEN-EN 12457[37] using deionized water with a liquid to solid ratio of 10. The mixture was placed in plastic bottles and shaken continuously for 24 h at 21 ± 2ºC. After the experiment, the liquids were filtered through a 0.2 μm polyether sulfone membrane and stored at 5°C after acidifying with nitric acid (65% suprapure) to prevent precipitation. Before acidification, the pH was measured. An ICP-OES spectrometer (Spectroblue FMX36) was used for the quantitative analysis of the leachate.

3 | RESULTS

3.1 | Bulk chemical and mineralogical composition

The mineralogical composition of the air granulated converter slag size fractions is given in Table 1. The standard

TABLE 1 Mineralogical composition of granulated converter slag without contaminants in wt%. The complete quantification is given in Table A1 in Appendix 1

Phase	Formula	2-4 mm	1-2 mm	0.5-1 mm	0.25-0.5 mm
Larnite, β-C_2S	Ca_2SiO_4	22 ± 0.5	19.4 ± 0.5	14.5 ± 0.5	8.1 ± 0.7
α_H'-C_2S	Ca_2SiO_4	21.9 ± 0.9	22 ± 0.9	27.6 ± 1.0	25 ± 1.6
Mg-Wuestite	(Fe,Mg)O	15.5 ± 1.2	15.4 ± 0.9	15.5 ± 0.8	13.5 ± 0.4
Srebrodolskite	$Ca_2(Fe,Al)_2O_5$	25.2 ± 0.3	22 ± 0.3	21.7 ± 0.3	16.5 ± 0.5
Perovskite	$CaTiO_3$	7.9 ± 0.2	10.3 ± 0.2	13.1 ± 0.2	11.1 ± 0.3
Magnetite	Fe_3O_4	2.6 ± 0.1	2.1 ± 0.1	2.9 ± 0.1	8.7 ± 0.3
Pseudobrookite	Fe_2TiO_5	0.3 ± 0.1	0.3 ± 0.1	0.3 ± 0.1	0.1 ± 0.1
Lime	CaO	0.1 ± 0.1		0.1 ± 0.1	
Protoenstatite	$Mg_2Si_2O_6$	1.3 ± 0.1	0.7 ± 0.2		
Naquite	FeSi	0.7 ± 0.1	0.5 ± 0.1	0.6 ± 0.1	0.4 ± 0.1
Titanite	$CaTiSiO_5$				0.6 ± 0.1
Rutile	TiO_2	0.4 ± 0.1	0.4 ± 0.1	0.5 ± 0.1	
Amorphous		2.1 ± 1.8	7 ± 1.5	3.1 ± 1.8	15.9 ± 1.4
$Ca_2(Fe,Al)_2O_5$ + $CaTiO_3$		33.1	32.3	34.8	27.6

Note: The Rwp value for all quantifications was between 7.4 and 7.9.

converter slag phases C_2S, (Fe,Mg)O, and srebrodolskite ($Ca_2(Fe,Al)_2O_5$)[2,6] were detected. C_2S is present as the α_H' and β polymorph in all granulated slag fractions, which is commonly the case in industrially cooled converter slag.[6] In addition, several new phases were identified: perovskite $CaTiO_3$, pseudobrookite Fe_2TiO_5, rutile TiO_2, titanite $CaTiSiO_5$, protoenstatite (Mg,Fe)SiO_3, and naquite FeSi. There were also phases present, especially in the smallest fraction, that are not converter slag minerals, for example quartz SiO_2, calcite $CaCO_3$, or corundum Al_2O_3. The presence of corundum is an artifact of the sample preparation with the McCrone XRD mill (Retsch), using corundum grinding elements. The other phases likely became mixed with the granulated slag while collecting the granules in the slag yard. Calcite and vaterite are also weathering products of converter slag. To compare the fractions with each other, the contamination phases were removed, and the rest recalculated to 100 wt%. Table 1 and Figure 2 show the results, the original quantification including contaminants is given in Table A1 in Appendix 1. It should be noted that the slag contains almost no free lime.

The three largest granulated slag fractions are very similar. The overall C_2S content is the same (41 to 44 wt%), but the β-C_2S content in the granulated converter slag increases with increasing granulated slag size fraction, while the α_H'-C_2S decreases (from 28 to 22 wt%). This is likely an effect of the slower cooling of the larger slag fractions, which allows for the transformation of more α_H'-C_2S, which is stable at higher temperatures, into β-C_2S. Only γ-C_2S is stable at room temperature, but the other high-temperature polymorphs can be stabilized by rapid cooling and the incorporation of minor ions.[38,39] The srebrodolskite ($Ca_2(Fe,Al)_2O_5$) content increases with increasing fraction size, while the perovskite ($CaTiO_3$) content decreases. The Srebrodolskite ($A_2B_2O_5$) structure can be regarded as an anion-deficient analog of perovskite (ABO_3) and a solid solution between both minerals exists[40] that can be described by the exchange mechanism $Fe^{3+}(B)+0.5\square(O) \leftrightarrow Ti^{4+}(B)+0.5O^{2-}(O)$ in conjunction with the simplified endmember components $Ca(A)Fe(B)O_{2.5}$ and $Ca(A)Ti(B)O_3$. The larger slag fractions cool slower, which gives srebrodolskite more time to form. This also fits with the observation that the sum of srebrodolskite and perovskite stays roughly the same in the three largest fractions (32 to 35 wt%). The amorphous content of the three largest granulated slag fractions is low overall and follows no clear trend.

The smallest granulated slag fraction (0.25-0.5 mm) contains a noticeably lower amount of β-C_2S, while the amorphous content is much higher than in the other fractions (15.9 wt%). This could indicate that the amorphous phase is generated during air granulation; however, this value is not reliable because the sample is contaminated with blast furnace slag, which is amorphous (Figure 2). The high content of magnetite (Fe_3O_4) indicates that this fraction is more oxidized than the larger ones due to the higher surface area that comes in contact with air during cooling. Iwasaki[8] discusses the effect of oxidation on converter slag and also mentions the formation of magnetite as well as a srebrodolskite/perovskite solid solution. No C_3S and practically no free lime (CaO) was detected in the samples. The absence of these phases could simply be a matter of an inappropriate chemical composition of the slag for crystallization of these phases. However, 1-2 wt% free lime commonly forms in converter steel slags at near-solidus conditions,[41,42] which may have been avoided with the rapid fractional crystallization occurring during air granulation.

TABLE 2 Chemical bulk composition of air granulated converter slag size fractions measured with XRF

Fraction	MgO	Al_2O_3	SiO_2	P_2O_5	CaO	TiO_2	V_2O_5	Cr_2O_3	MnO	Fe_2O_3	LOI	GOI
2-4 mm	8.97	2.01	15.5	1.53	45.6	1.49	0.64	0.18	4.22	20.5		0.78
1-2 mm	8.78	2.10	15.4	1.53	45.3	1.48	0.63	0.18	4.19	20.6		0.46
0.5-1 mm	8.51	2.97	15.3	1.49	44.0	1.48	0.62	0.17	4.08	21.1	0.18	
0.25-0.5 mm	5.82	7.90	19.9	1.00	30.4	1.16	0.43	0.15	2.74	24.9	5.60	

Note: All results are in wt%.

The bulk chemical composition of all air granulated converter slag fractions is given in Table 2. The two largest fractions show a small gain on ignition due to the oxidation of Fe^{2+} to Fe^{3+}, while the two smallest fractions lost weight, mainly due to the decomposition of calcite.[43] Around 2/3 of the total iron content in the slag is Fe^{2+}, the rest is present as Fe^{3+}. Table 1 only shows the amount of Fe_2O_3, because fused beads were made for the XRF analysis and the process oxidizes all Fe^{2+} to Fe^{3+}. Chemically the 2-4 mm, 1-2 mm, and 0.5-1 mm fractions of air granulated converter slag are very similar and well within the range of industrially cooled converter slag reported in the literature.[6,9,32] The 0.25-0.5 mm fraction however shows a much higher Al_2O_3 and SiO_2 content, while CaO and MgO are lower. The SiO_2 content is likely influenced by the 8.9 wt% quartz contained in the sample (Appendix 1, Table A1), while the deviating Al_2O_3, CaO, and MgO contents are caused by the presence of amorphous contaminants such as blast furnace slag (Figure 2).

3.2 | Microstructure and mineralogy determined by large area phase mapping

In order to study the influence of rapid cooling on the microstructure and composition of the mineral phases, large area SEM/EDX phase mapping was carried out using PARC. The results for the 2-4 and the 0.25-0.5 mm fraction are given in Figures 1 and 4, respectively. The phase maps of the other two fractions are shown in the Appendix 1 (Figures A1 and A2). Granules of the same size developed strikingly similar crystallization microstructures and only one granule is described here in detail to highlight the characteristic features of its size fraction. All granulated slag fractions contained large crystals of C_2S and (Mg,Fe)O that are embedded in a fine-grained matrix that is a mix of different minerals with a size below the EDX resolution of 1 µm. Similar observations were made by other researchers.[9,32] Based on variation in Ca – Si composition, the matrix was divided into 3 groups using a density plot (Figure 3). These groups were named Matrix CF (CaFe), CS (CaSi), and MF (MgFe) according to the major elements present. Very small amounts of CaO and (Ca,Mg)O phase were also detected. The area% of each phase is given in Figure 5a), the average chemical composition of the major phases in Figures 4 and 7c-e. The results are free from the influence of contaminants because only SI fields containing converter slag grains were analyzed.

There is a clear correlation between slag size fraction and phase content in area%. The largest fraction (2-4 mm) contained the highest amount of C_2S and the lowest total amount of matrix phase, while the opposite was true for the smallest fraction (0.25-0.5 mm). The 0.25-0.5 mm fraction also contained the largest amount of the calcium and silica-rich Matrix CS, which reduced with increasing size fraction (Figure 5a). This is a clear indication that lower cooling speeds allow for the growth of C_2S out of this matrix part. This is also corroborated by the microstructure itself (Figure 6). In the 0.25-0.5 mm fraction, the C_2S is present as large, round phenocrysts. They form in the liquid slag before granulation at temperatures of around 1,550°C[9] and can be regarded as equilibrium crystallization. In the larger slag fractions, the C_2S

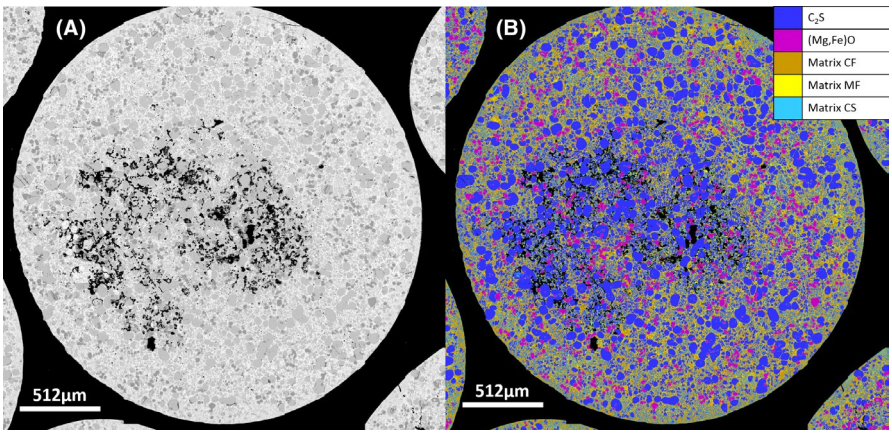

FIGURE 1 Air granulated converter slag 2-4 mm (A) SEM grayscale image (B) Phase map

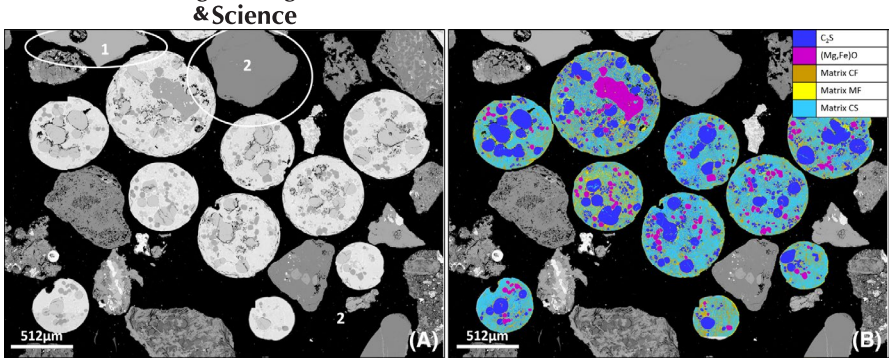

FIGURE 2 Air granulated converter slag 0.25-0.5 mm surrounded by other grains (A) SEM grayscale image 1- blast furnace slag 2- quartz (B) Phase map

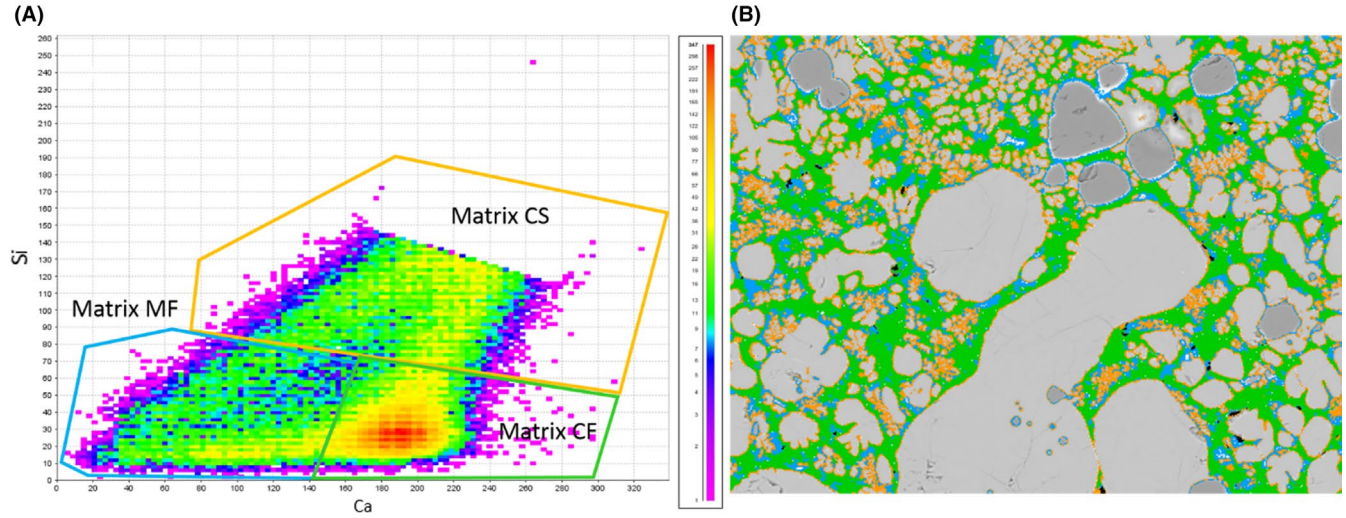

FIGURE 3 A, PARC density plot for all data points belonging to the matrix phase and their division into 3 matrix parts. The intensity of the Ca Kα peak is plotted against the intensity of Si Kα, and the color indicates the density of overlapping data points. B, Corresponding areas in a SI data field of air granulated converter slag

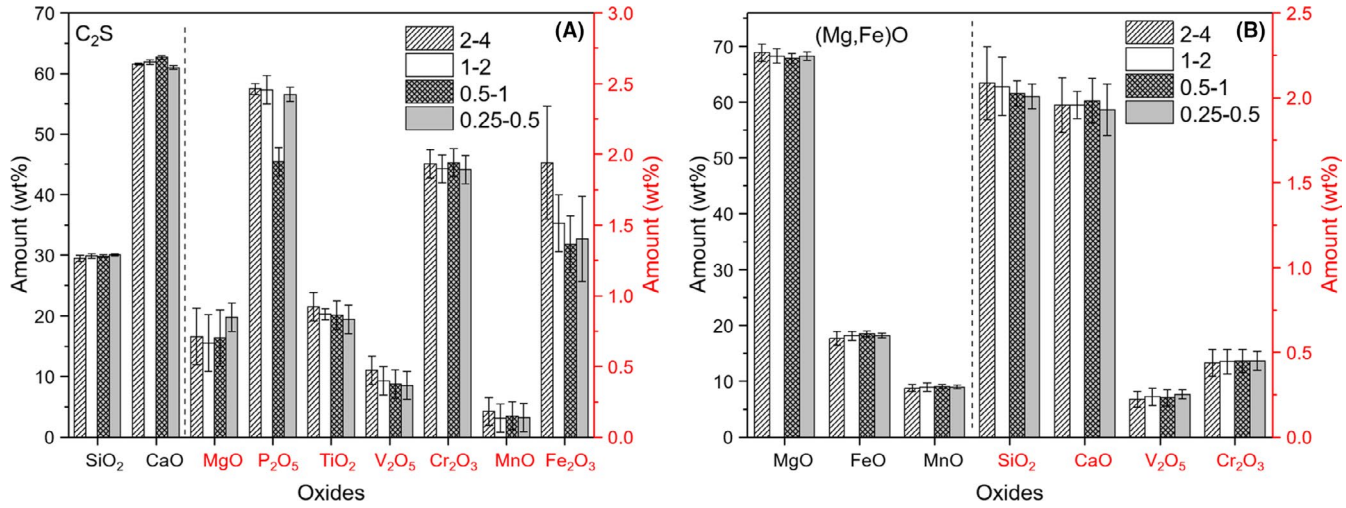

FIGURE 4 Average composition of (A) C_2S and (B) (Mg,Fe)O phenocrysts related to the grain size of the air granulated converter slag. Note the difference in scale for major and minor oxides

shows leaf-like shapes that are formed during granulation and can be regarded as quench crystallization because they form after the equilibrium C_2S during cooling. These shapes are likely connected, three-dimensional structures in the slag. It should be noted that PARC cannot differentiate between C_2S polymorphs, because their chemistry is the same.

The composition of C_2S (Figure 4) changes with increasing slag size fraction and becomes more iron-rich. The V_2O_5

(A)

	Fraction	C2S	(Mg,Fe)O	CaO	(Mg,Ca)O	Matrix		
						CF	MF	CS
Area%	2-4mm	43.9	6.7	0.5	0.3	27	9.2	12.5
	1-2mm	40.5	6.2	0.5	0.3	24.5	8.7	19.2
	0.5-1mm	29	6.7	0.4	0.5	23.8	11.5	28.1
	0.25-0.5mm	21.1	10.3	0.4	0.4	16.2	6.5	45
wt%	2-4mm	39.5	7.9	0.6	0.4	28.0	12.5	11.2
	1-2mm	36.7	7.3	0.6	0.4	25.6	12.0	17.4
	0.5-1mm	26.1	7.9	0.5	0.6	24.7	15.1	25.3
	0.25-0.5mm	19.5	12.4	0.5	0.5	17.2	8.4	41.6
	Density (g/cm³)	3.3	4.2	3.3	3.4	3.8	4.3	3.3

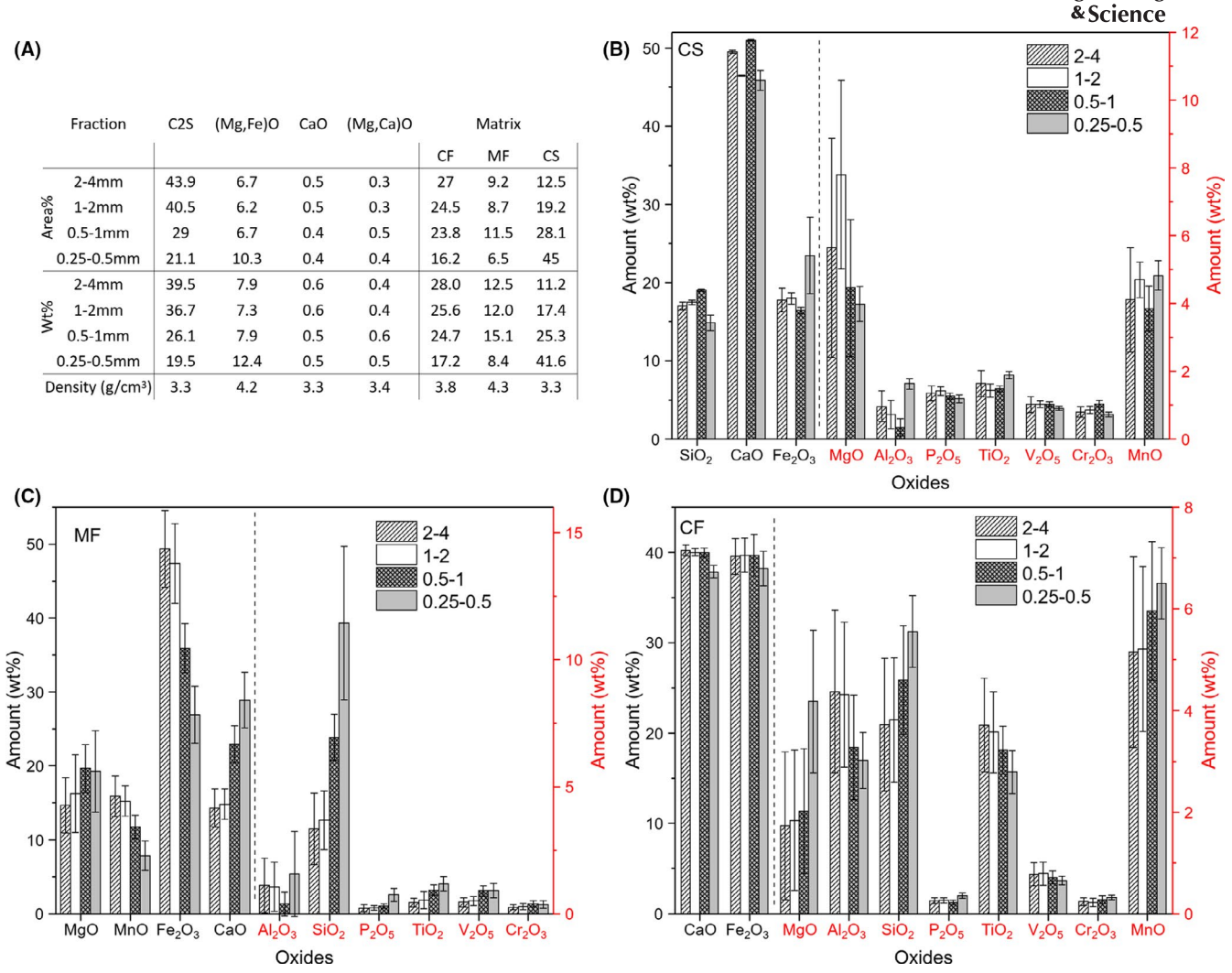

FIGURE 5 Results of PARC analysis (A) Phases in air granulated converter slag in area% and wt% including the densities used for conversion from area% into wt% (B) Composition of the CS matrix part (C) Composition of the MF matrix part (D) Composition of the CF matrix part. Note the difference in scale for major and minor oxides

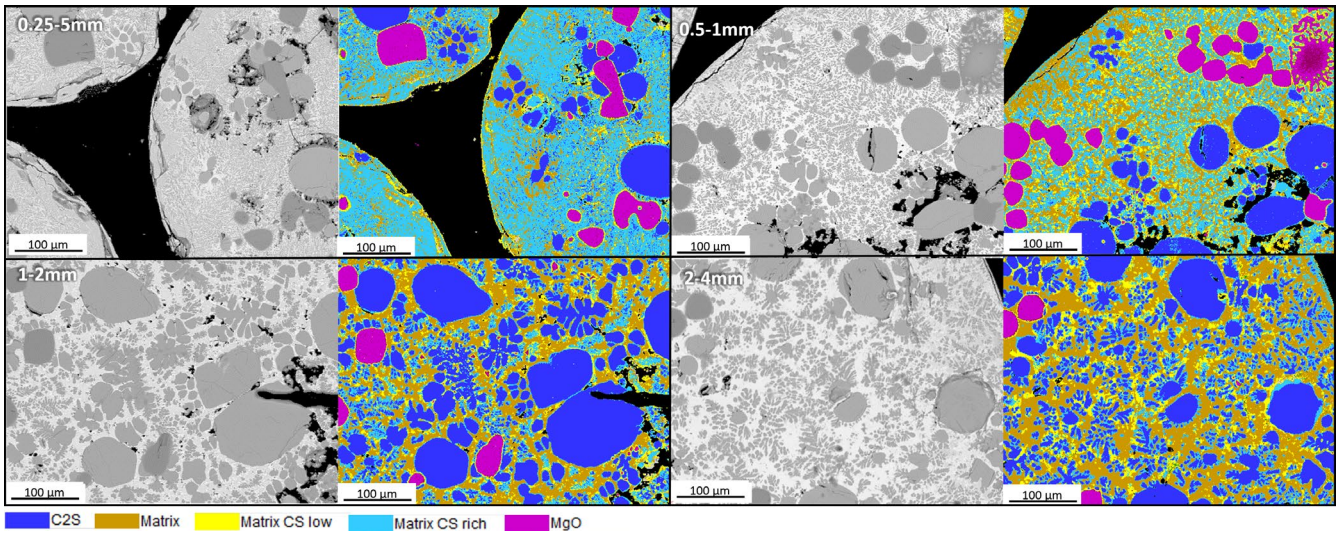

FIGURE 6 Formation of C_2S out of the CS rich matrix with increasing air granulated converter slag size fraction/decreasing cooling speed. The C_2S present in the 0.25-0.5 mm fraction is the equilibrium C_2S formed before granulation. The quench C_2S forming during cooling shows a leaf-like structure

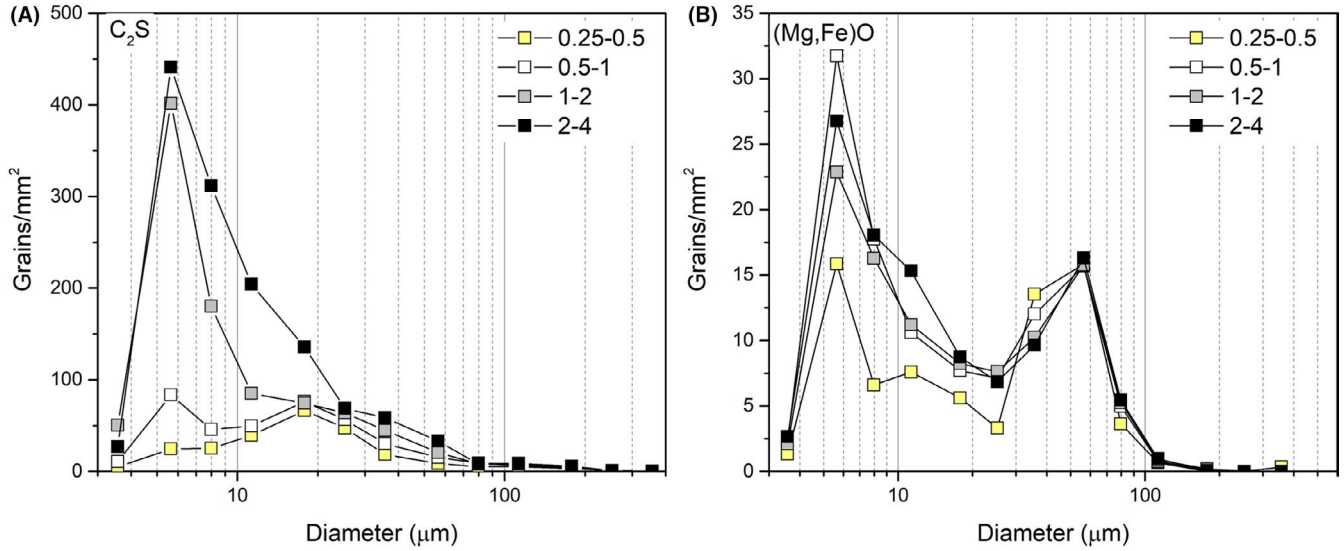

FIGURE 7 Size distribution of (A) C_2S and (B) (Mg,Fe)O crystals in air granulated converter slag. The diameter is calculated from the grain area assuming perfect circular shape. The amount of grains is normalized by the total grain area measured

and TiO_2 contents also increase slightly, because the quench C_2S incorporates more minor ions as the composition of the liquid slag changes during cooling.[44] We are aware that the Cr_2O_3 content in the C_2S is higher than the true value by about an order of magnitude due to the Si + Ca sum peak in the C_2S spectrum overlapping with the Cr Kα emission line.

No C_3S was formed based on the microstructure of the granulated slag. C_3S forms at higher temperatures than C_2S as well-defined euhedral crystals but requires a more calcic slag composition. These C_3S crystal shapes are preserved during cooling even if the C_3S itself converts to C_2S and CaO.[6,45]

Most equilibrium C_2S phenocrysts in the smallest granulated slag fraction have a diameter of around 9 μm (see Chapter 2.2) (Figure 7a). It can be assumed that this is very close to the average size the phenocrysts had in the liquid slag before cooling, because the smallest fraction cools so quickly that there is little time for further (quench) C_2S to form. With increasing fraction size many small grains (around 2 μm in diameter) appear due to the formation of quench C_2S in leaf-like shapes. At the same time, the number of very large (15-30 μm) C_2S phenocrysts increases slightly. This shows that C_2S continues crystallizing and growing during cooling. The bigger granulated slag fractions cool slower and allow more time for the leaf-like patterns to form. This quench C_2S also grows on the equilibrium phenocrysts increasing their average size. According to the XRD results, the α'-C_2S content changes very little in the different granulated slag sizes. However, the β-C_2S content increases with increasing droplet size, which indicates that the quench C_2S in the leaf-like patterns is largely β-C_2S. The exact cooling rate of the granulated slag fractions is unknown, but the amount of quench C_2S is similar to that observed by Gautier et al.[9], who used water quenching and estimated a cooling time of 3-5 s. It is likely that water quenching is less effective for rapid cooling of converter slag than for blast furnace slag due to its self-insulating properties. The cooling speeds of air and water granulation could therefore be in a similar range.

(Mg,Fe)O is the other phenocryst phase present in the air granulated converter slag. Calculations with FactSage (a software suite for thermodynamic calculations) show that it starts crystallizing at around 1,840°C for this slag composition. Some C_2S phenocrysts in the samples contained (Mg,Fe)O inclusions showing that it forms at higher temperatures than the C_2S (Figure 6, 0.5-1 mm). This order of crystallization was also found by other researchers.[9] The (Mg,Fe)O content in the 3 largest granulated converter slag fractions was between 6.2 and 6.7 area%, while the 0.25-0.5 mm fraction contained 10.3 area% (Figure 5a). The equivalent values in wt% are also given in Figure 5a. There is a clear correlation between the size fraction and phenocryst size distribution (Figure 7b). The smallest granulated slag fraction (0.25-0.5 mm) shows a bimodal distribution with maxima at around 3 and 25 μm. This may be due to the fact that some of the (Mg,Fe)O is present as small inclusions in the C_2S, which are prevented from further growth during cooling of the slag. With increasing droplet size, the first maximum increases in intensity showing that new, small (Mg,Fe)O is formed with decreasing cooling speed. The size of the largest (Mg,Fe)O phenocrysts remains largely unchanged, however.

The amount of matrix decreases with increasing droplet size and decreasing cooling speed from around 68 area% (0.25-0.5 mm) to 49 area% (2-4 mm). As discussed previously, the Matrix CS part forms C_2S but does not change its average composition with changing cooling speed (Figure 5b). There is also a clear increase in the amount of Matrix CF with slower cooling. This matrix part is rich in CaO and Fe_2O_3 (Figure 5d) and contains the majority of

Al_2O_3 and TiO_2 present in the slag. Based on the composition, this PARC phase contains the srebrodolskite ($Ca_2(Fe,Al)O_5$) detected in XRD together with the other TiO_2 bearing phases (Table 1, Figure 2). Srebrodolskite ($Ca_2(Fe,Al)O_5$) is the last phase to form during standard cooling of converter slag, as can be seen from the texture of industrially cooled slag. More Matrix CF is generated the slower the granulated slag cools, while its average composition changes only slightly. With increasing size, it becomes richer in Al_2O_3 and TiO_2, while the MgO, SiO_2, and MnO content decreases.

The amount of MF matrix (6.5-11.5 area%) shows no clear correlation with the slag fraction size but has the greatest variation in composition. The iron and manganese content decreases with decreasing slag size, while the CaO, SiO_2, and MgO contents increase. Based on this trend, it can be assumed that (Mg,Fe)O grows out of this matrix phase during cooling. The formation of new (Mg,Fe)O can also be seen in the phenocryst size distribution (Figure 7b).

Converter steel slag is generated in batches and can be quite variable in composition, depending on the quality of steel produced. However, the general crystallization behaviors described here are expected to apply to other slag compositions as well, especially those that contain little free lime, even if the phase proportions may be different.

3.3 | Influence of granulation on phase distribution and chemical bulk composition

It is possible to calculate the chemical bulk composition of each granulated converter slag fraction out of the PARC data if the phases are converted from area% into wt% using their densities (Figure 5a). For C_2S and (Mg,Fe)O the appropriate density can be taken directly from the Rietveld refinement results. They are 3.3 and 4.3 g/cm^3, respectively. Assigning a density to the three matrix phases is less straightforward because they are a mix of different minerals. However, it is clear that the Matrix CS phase reacts to C_2S during cooling, the Matrix MF phase contains mostly (Mg,Fe)O and that the Matrix CF phase is very rich in srebrodsolskite ($Ca_2(Fe,Al)O_5$). For this reason, they can be assigned the densities of C_2S, (Mg,Fe)O and srebrodolskite (3.8 g/cm^3 based on Rietveld refinement), respectively. The phase composition in wt% can be seen in Figure 5a) and the calculated bulk composition in Table 3. For the three biggest fractions, the measured XRF bulk composition (Table 2) matches the calculated bulk composition very well, but there is a big difference for the 0.25-0.5 mm fraction due to the contamination with other minerals. It is also clear that the Cr_2O_3 content is overestimated by an order of magnitude in the calculated composition for reasons explained before. But this does not influence the other oxide amounts in any significant way.

This calculated chemical bulk composition has the advantage of being free from contaminant influence because nonslag phases can be excluded from phase mapping with PARC, even if they are amorphous. It also shows that the deviating bulk composition of the 0.25-0.5 mm granulated slag fraction is not just an effect of contamination. This is unexpected because all slag fractions were derived from the same converter slag batch. The likely explanation is an uneven distribution of the C_2S and (Mg,Fe)O phenocrysts in the different droplets, which affects their bulk composition. To visualize if accumulation/depletion of phenocrysts is the cause of the compositional differences, variation diagrams have been constructed in which the element-oxide components are plotted against CaO (Figure 8). In these diagrams, the bulk composition of each converter slag fraction is represented as well as the compositions of the (Mg,Fe)O and C_2S phenocrysts (Figure 4). Element oxides that lie on a straight line indicate a compositional relationship derived by the addition or subtraction of C_2S and (Mg,Fe)O phenocrysts respectively. Relative proportions of each phase can be calculated with a lever-rule approach. $Oxide_{(Mg,Fe)O}$/$Oxide_{C2S}$ is the oxide concentrations in the (Mg,Fe)O and C_2S phenocrysts as determined with PARC (Figure 4).

The variation diagrams show that the composition of the three largest granulated slag fractions is consistent with the composition of the smallest slag fraction (0.25-0.5 mm) containing more (Mg,Fe)O (in the range of 5 to 10 wt%). If C_2S is added to the 0.25-0.5 mm fraction instead, the Fe_2O_3 and SiO_2 concentrations of the larger slag fraction are relatively far outside the range. This means the different composition of the smallest slag fraction is likely caused by an enrichment of (Mg,Fe)O phenocrysts and not by a lack of C_2S. The reason for this is unclear but may be connected to the bimodal size distribution of the (Mg,Fe)O or the granulation process itself.

TABLE 3 Chemical bulk composition of air granulated converter slag size fractions determined via PARC

Size	MgO	Al_2O_3	SiO_2	P_2O_5	CaO	TiO_2	V_2O_5	Cr_2O_3	MnO	Fe_2O_3
2-4 mm	8.7	1.5	15.2	1.2	43.4	1.7	0.60	1.0	4.7	21.7
1-2 mm	9.1	1.4	15.6	1.2	43.4	1.6	0.61	1.0	4.7	21.1
0.5-1 mm	10.2	1.0	15.0	0.9	43.1	1.5	0.69	0.9	5.0	21.5
0.25-0.5 mm	12.6	1.3	14.2	1.1	40.5	1.5	0.66	0.8	4.9	21.5

Note: All results are given in wt%.

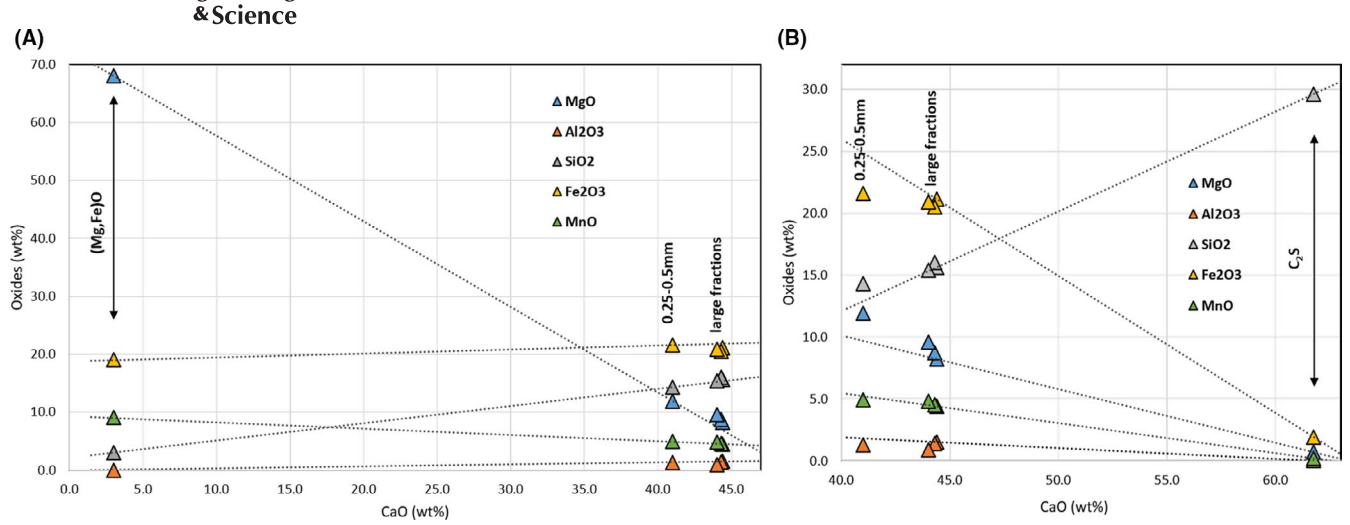

FIGURE 8 Variation diagram A) Addition of (Mg,Fe)O B) Addition of C_2S to air granulated converter slag

3.4 | Vanadium and chromium leaching

The environmental properties of the converter slag were measured using the one batch leaching test, and the results are shown in Table 4 along with the pH of the leachate. Chromium and Vanadium are the only elements above the legal limit defined in the Dutch Soil Quality degree for all fractions and much higher than observed for normal industrially cooled slag. This is likely the result of an increased solubility of the slag due to air granulation, which releases Chromium and Vanadium. Vanadium leaching decreases with decreasing slag size, while chromium leaching increases. However, these leaching results are also influenced by the presence of contaminants such as quartz and calcite. These contaminant phases do not contain V and Cr and effectively reduce the amount of slag in the sample as well as the pH. The 0.25-0.5 mm fraction contains the highest amount of contaminants and has the lowest pH (9.6). But since the amount of crystalline contaminants is known from XRD (Appendix 1, Table A1), an attempt can be made to correct the leaching values (Table 4). In these corrected values, the vanadium leaching turns out very similar for all granulated slag droplet fractions (11.03 to 11.83 mg/kg_{ds}), while the Cr leaching still increases with decreasing slag size fraction (from 1.75 to 3.05 mg/kg_{ds}). Table 5 shows how much of the total V_2O_5 and Cr_2O_3 present in the slag this represents. It also shows the distribution of both oxides between C_2S, MgO, and the matrix. The total leachable amount of V_2O_5 reduces slightly with decreasing slag size. At the same time, we also see a decrease of the V_2O_5 bound in C_2S as the result of a lower C_2S content in the smaller granules. It is likely that both, C_2S and the matrix, leach V_2O_5, but that C_2S contributes more. The high leaching of vanadium therefore indicates an increased solubility of C_2S in water compared with industrially cooled slag. If this is the case, it can be expected that C_2S hydrates when used as a cement replacement material and could show similar properties to belite cement.[46]

TABLE 4 Leaching data ICP analysis of the one batch leaching test and pH of the leachate

		Measured values							
	pH	11		10.8	10.9	9.6	Corrected values		
Element[a]	Legal limit	2-4 mm	1-2 mm	0.5-1 mm	0.25-0.5 mm		2-4 mm	1-2 mm	0.5-1 mm	0.25-0.5 mm
Sb	0.32	0.19	0.19	0.17	0.18		0.20	0.19	0.18	0.23
As	0.9	0.21	0.22	0.15	0.15		0.22	0.22	0.16	0.19
Ba	22	0.11	0.02	0.02	0.11		0.11	0.02	0.02	0.14
Cr	0.63	1.7	1.83	1.91	2.42		1.75	1.86	1.98	3.05
Mo	1	0.14	0.14	0.002	0.011		0.14	0.14	0.00	0.01
V	1.8	11.49	10.84	11.43	8.84		11.83	11.03	11.82	11.13
Zn	4.5	0.06	0.06	0.07	0.08		0.06	0.06	0.07	0.10

Note: The legal limit is the limit set by the Dutch Soil Quality Degree for unbound material. Left measured value, right values corrected for contaminants. All results in mg per kg of dry solid sample.

[a]Cu, Co, Hg, Ni, Se, Cd, Pb and Sn were below the detection limit.

TABLE 5 Total amount of V_2O_5 (from PARC bulk composition) and Cr_2O_3 (from XRF bulk composition) in granulated converter slag, the amount leachable from the slag, and the distribution of these oxides between the host phases C_2S, matrix and (Mg,Fe)O (from PARC)

V_2O_5						Cr_2O_3					
	Total	Leachable	C_2S	Matrix	MgO		Total	Leachable	C_2S	Matrix	MgO
Size	(wt%)	(%)	(%)	(%)	(%)	Size	(wt%)	(%)	(%)	(%)	(%)
2 mm	0.60	0.70	31.4	66.1	2.5	2 mm	0.18	0.26	77.6	19.5	2.9
1 mm	0.61	0.65	24.2	73.2	2.5	1 mm	0.18	0.27	71.8	25.3	3.0
0.5 mm	0.68	0.62	15.0	82.3	2.6	0.5 mm	0.17	0.29	55.1	41.3	3.6
0.25 mm	0.66	0.60	11.4	84.0	4.6	0.25 mm	0.15	0.45	46.6	46.8	6.6

The leachable amount of the total Cr_2O_3 content in the slag fractions clearly increases with decreasing slag size from 0.26% to 0.45%. As discussed before, the content of Cr_2O_3 in C_2S is systematically overestimated, but the trend in the distribution between the 3 phases shown in Table 5 is still useful and seems to indicate that the matrix is contributing the majority of leached Cr_2O_3.

4 | CONCLUSION AND OUTLOOK

Air granulated converter slag was divided into four different size fractions (0.25-0.5 mm, 0.5-1 mm, 1-2 mm, and 1-4 mm) to study the influence of granule size and therefore cooling speed on the mineralogy of converter slag. The three largest fractions are very similar in chemical and mineralogical composition, with a total Ca_2SiO_4 (C_2S) content of 41-44 wt% and very little amorphous phase.

The smallest granulated converter slag fraction (0.25-0.5 mm) is markedly different in composition. It contains less Ca_2SiO_4 and shows the highest amorphous content (15.5 wt%), which may be caused in part by contamination with blast furnace slag. This fraction is the most oxidized and contains large amounts of magnetite (Fe_3O_4). The chemical bulk composition also shows it contains more MgO and less CaO and SiO_2.

All granulated slag fractions contain phenocrysts of Mg-wuestite ((Fe,Mg)O) and C_2S that are embedded in a finely grained matrix that formed during cooling. No individual mineral phases can be discerned in the matrix due to their small size (<1μm). The smallest slag fraction contains 5%-10% more (Fe,Mg)O phenocrysts, which is also responsible for the difference in bulk composition. However, the starting composition was the same for all fractions. Further investigation is required to understand this phenomenon.

The fine-grained matrix of the granulated slag can be divided into three types based on the composition: Ca/Si-rich, Ca/Fe-rich, and Mg/Fe-rich. The amount of Ca/Si-rich matrix reduces with decreasing cooling speed/ increasing granule size and forms quench Ca_2SiO_4 in the form of leaf-like patterns. The Ca/Fe-rich matrix type contains the majority of Al_2O_3 and TiO_2 and therefore the srebrodolskite and perovskite. The Mg/Fe-rich matrix has a highly variable composition, containing less MnO and Fe_2O_3 with decreasing slag size and is assumed to be the source of additional Mg-wuestite that forms during cooling.

All slag fractions leach more Cr and V than industrially cooled converter slag and surpass the legal limit defined by the Dutch Soil Quality degree. The V leaching is very similar for all fractions, while the Cr leaching increases with decreasing slag size. The main sources of these elements are Ca_2SiO_4 and the matrix phase. The increased V and Cr leaching indicate that granulated converter slag is more soluble in water than industrially cooled slag.

The results show that it is not possible to create amorphous converter slag using air granulation. But even if sufficiently rapid cooling is applied, around 30 wt% of the slag would remain crystalline, due to the formation of solid Ca_2SiO_4 and Mg-wuestite before cooling. However, the air granulation may have suppressed the near-solidus crystallization of free lime. The absence of free lime would circumvent the problem of volume expansion caused by its hydration.

The leaching results indicate a higher solubility of Ca_2SiO_4 in water and therefore the potential for a higher hydraulic reactivity. Converter steel slag should therefore not be compared with granulated blast furnace slag, which is an amorphous, pozzolanic material that requires a high pH solution to contribute strength in binder systems (eg, CEMIIIb). Instead, it should be compared to cement that hardens in the presence of water alone and generates its own high pH pore solution. In this case, a high amount of amorphous phase is not a prerequisite for reactive granulated converter steel slag. Further research into the cementitious properties is currently ongoing, but it seems that an application as a partial cement replacement has great potential and could make it possible to recycle all steel slag in the future. It may also solve the problematic leaching of V and Cr, as the hydration products of cement have a high binding capacity for heavy metals.

ACKNOWLEDGMENTS

The authors want to thank Corrie van Hoek and Frank van der Does at Tata Steel Ijmuiden for carrying out measurements, preparing samples, and technical discussions.

ORCID

Katrin Schollbach https://orcid.org/0000-0002-9945-6467

REFERENCES

1. Dippenaar R. Industrial uses of slag (the use and re-use of iron and steelmaking slags). Ironmak Steelmak. 2005;32(1):35–46.
2. Waligora J, Bulteel D, Degrugilliers P, Damidot D, Potdevin JLL, Measson M. Chemical and mineralogical characterizations of LD converter steel slags: A multi-analytical techniques approach. Mater Charact. 2010;61(1):39–48.
3. World Steel Association. Steel industry co-products – worldsteel position paper [Internet]. 2018. Available from: worldsteel.org
4. Eurofer. European Steel in Figures [Internet]. http://Eurofer.eu/20190 7-SteelFigures.pdf Accessed January 2020. 2019. Available from: http://Eurofer. eu/201907-SteelFigures.pdf Accessed January 2020.
5. Fisher LV, Barron AR. The recycling and reuse of steelmaking slags — A review. Resour Conserv Recycl. 2019;146(April):244–55.
6. van Hoek C, Small J, van der Laan S. Large-area phase mapping using phase recognition and characterization (PARC) software. Micros Today. 2016;24(5):12–21.
7. Chaurand P, Rose J, Briois V, Salome M, Proux O, Nassif V, et al. New methodological approach for the vanadium K-Edge X-ray absorption near-edge structure interpretation: application to the speciation of vanadium in oxide phases from steel slag. J Phys Chem B. 2007;111(19):5101–10.
8. Iwasaki I, Fregeau-Wu E, Fujita T. Removal of phosphorus from steelmaking slags: a literature survey. Miner Process Extr Metall Rev. 1993;12(1):19–36.
9. Gautier M, Poirier J, Bodénan F, Franceschini G, Véron E. Basic oxygen furnace (BOF) slag cooling: Laboratory characteristics and prediction calculations. Int J Miner Process. 2013;123:94–101.
10. Engström F, Adolfsson D, Yang Q, Samuelsson C, Björkman B. Crystallization behaviour of some steelmaking slags. steel Res Int. 2010; 81(5):362–71.
11. Braconi A. SESSION III: CASE STUDIES AND VIEWS FROM OTHER METAL SECTORS & CONCLUSIONS LEGAL FRAMEWORK AND SECONDARY RAW MATERIALS: STEEL VIEWS AND EXAMPLES EUROFER-Circular Economy & Raw Material, Senior Manager Thomas Reiche EUROSLAG-Chairman/FEhS-Institute, Mana.
12. Moon HY, Yoo JH, Kim SS. A fundamental study on the steel slag aggregate for concrete. Geosystem Eng. 2002;5(2):38–45.
13. Maharaj C, White D, Maharaj R, Morin C. Re-use of steel slag as an aggregate to asphaltic road pavement surface. Cogent Eng. 2017;4(1).
14. Chaurand P, Rose J, Briois V, Olivi L, Hazemann J-LL, Proux O, et al. Environmental impacts of steel slag reused in road construction: A crystallographic and molecular (XANES) approach. J Hazard Mater. 2007;139(3):537–42.
15. Juckes LM. The volume stability of modern steelmaking slags. Miner Process Extr Metall. 2003;112(3):177–97.
16. Liu F, Chen MZ, Li FZ, Li QL, Wu SP, Sang Y. Effect of ground steel slag powder on cement properties. Mater Res Innov. 2015;19:S1150–S1153.
17. Lu TH, Chen YL, Shih PH, Chang JE. Use of basic oxygen furnace slag fines in the production of cementitious mortars and the effects on mortar expansion. Constr Build Mater. 2018;167:768–74.
18. Cheng H, Yi H, Wang J, Wan Y, Xu G, Chen H. An Overview of Utilization of Steel Slag. Procedia Environ Sci. 2012;16:791–801.
19. Jiang Y, Ling TC, Shi C, Pan SY. Characteristics of steel slags and their use in cement and concrete—A review. Resour Conserv Recycl. 2018;136(December 2017):187–97.
20. Guo J, Bao Y, Wang M. Steel slag in China: Treatment, recycling, and management. Waste Manage. (Oxford). 2018;78:318–30.
21. Takahashi T, Yabuta K. New applications for iron and steelmaking slag. NKK Tech Rev. 2002;87:38–44.
22. Liu G, Schollbach K, van der Laan S, Tang P, Florea MVA, Brouwers HJH. Recycling and utilization of high volume converter steel slag into CO2 activated mortars – The role of slag particle size. Resour Conserv Recycl. 2020;160:104883.
23. Wan J, Du H, Gao F, Wang S, Gao M, Liu B, et al. Direct Leaching of Vanadium from Vanadium-bearing Steel Slag Using NaOH Solutions: A Case Study. Miner Process Extr Metall Rev [Internet]. 2020;00(00):1–11.
24. van Zomeren A, van der Laan SR, Kobesen HBA, Huijgen WJJ, Comans RNJ. Changes in mineralogical and leaching properties of converter steel slag resulting from accelerated carbonation at low CO 2 pressure. Waste Manag. 2011;31(11):2236–44.
25. Circular Dutch economy by 2050 [Internet]. [cited 2020 Oct 1]. Available from: https://www.government.nl/topics/circular-economy/circular-dutch-economy-by-2050
26. European Commission. Circular Economy Action Plan: The European Green Deal. European Commission. 2020.
27. Zhang H, Wang H, Zhu X, Qiu Y-J, Li K, Chen R, et al. A review of waste heat recovery technologies towards molten slag in steel industry. Appl Energy [Internet]. 2013;112:956–66.
28. Tripathy SK, Dasu J, Murthy YR, Kapure G, Pal AR, Filippov LO. Utilisation perspective on water quenched and air-cooled blast furnace slags. J Clean Prod. 2020;262:121354.
29. Ökvist LS. High temperature properties of BOF slag and its behaviour in the blast furnace. Steel Res Int. 2004;75(12):792–9.
30. Taylor HFW. Cement chemistry, 2nd edn. London: Thomas Telford; 1997.
31. Choi M, Jung S-M. Crystallization behavior of melted BOF slag during non-isothermal constant cooling process. J Non Cryst Solids [Internet]. 2017;468:105–12. Available from http://www.sciencedirect.com/science/article/pii/S0022309317302326.
32. Tossavainen M, Engstrom F, Yang Q, Menad N, Lidstrom Larsson M, Bjorkman B. Characteristics of steel slag under different cooling conditions. Waste Manag. 2007;27(10):1335–44.
33. Gualtieri AF. Accuracy of XRPD QPA using the combined Rietveld-RIR method. J Appl Crystallogr. 2000;33(2):267–78.
34. Coelho AA *TOPAS* and *TOPAS-Academic* : an optimization program integrating computer algebra and crystallographic objects written in C++. J Appl Crystallogr. 2018;51(1):210–8.
35. Alam Q, Schollbach K, van Hoek C, van der Laan S, de Wolf T, Brouwers HJHJH, et al. In-depth mineralogical quantification of MSWI bottom ash phases and their association with potentially toxic elements. Waste Manag. 2019;87:1–12.
36. Schneider CA, Rasband WS, Eliceiri KW. NIH Image to ImageJ: 25 years of image analysis. Nat. Methods. 2012;9(7):671–5.
37. NEN-EN 12457 - Karakterisering van afval - Uitloging - Verkorte uitloogproef van korrelvormigeafvalstoffen en slib. 2002.
38. Rejmak P, Dolado JS, Aranda MAG, Ayuela A. First-Principles Calculations on Polymorphs of Dicalcium Silicate—Belite,

a Main Component of Portland Cement. J Phys Chem C. 2019;123(11):6768–77.
39. Fayon F, Duée C, Bodénan F, Allix M, Bourgel C, Poirier J, et al. Phosphorus speciation in dicalcium silicate phases: Application to the basic oxygen furnace (BOF) slag. Cem Concr Res. 2015;73:207–14.
40. Antipov EV, Abakumov AM, Istomin SY. Target-aimed synthesis of anion-deficient perovskites. Inorg Chem. 2008;47(19):8543–52.
41. Eisenhüttenleute VD, Allibert M, Gaye H, Geisler J, Janke D, Keene BJ, et al. Slag atlas. , Slag Atlas: Verlag Stahleisen; 1995.
42. Troemel G, Koch K, Fix W, Grosskurth N. Der Einfluss des magnesiumoxyds auf die Gleichgewichte im System Fe-CaO- FeO-SiO2 und die Schwefelverteilung bei 1600 C. Arch Eisenhuettenw. 1969;40:969–978.
43. Scrivener K, Snellings R, Lothenbach B. A Practical Guide to Microstructural Analysis of Cementitious Materials. A Practical Guide to Microstructural Analysis of Cementitious Materials. 2018.
44. Bodénan F, Gautier M, Rafai N, Poirier J, Piantone P, Franceschini G, et al. Phosphorus speciation in dicalcium silicate polymorphs of basic oxygen furnace (BOF) slag – Preliminary results. Déchets, Sci Tech. 2010;57:1–5.
45. Li X, Shen X, Tang M, Li X. Stability of tricalcium silicate and other primary phases in portland cement clinker. Ind Eng Chem Res. 2014;53(5):1954–64.
46. Staněk T, Sulovský P. Active low-energy belite cement. Cem Concr Res. 2015;68:203–210.

How to cite this article: Schollbach K, Ahmed MJ, van der Laan SR. The mineralogy of air granulated converter slag. *Int J Ceramic Eng Sci*. 2021;3:21–36. https://doi.org/10.1002/ces2.10074

APPENDIX 1

TABLE A1 Mineralogical composition of granulated converter slag

Phase	Formula	Type	>4 mm	Stdev.	2-4 mm	Stdev.	1-2 mm	Stdev.	0.5-1 mm	Stdev.	0.25-0.5 mm	Stdev.	<0.25 mm	Stdev.
Larnite, β-C_2S	Ca_2SiO_4	P	22.9	0.5	21	0.5	18.9	0.5	13.9	0.5	6.2	0.5	2.7	0.3
α'-C_2S	Ca_2SiO_4	P	16.5	1	20.9	0.9	21.4	0.9	26.4	1	19	1.2		
Mg-Wuestite	(Fe,Mg)O	P	17.1	1.5	14.8	1.1	15	0.9	14.8	0.8	10.2	0.3	5.9	0.2
Srebrodolskite	$Ca_2Fe_2O_5$	P	23.9	0.4	24.1	0.3	21.4	0.3	20.8	0.3	12.6	0.4	10.3	0.3
Perovskite	$CaTiO_3$	P	6.6	0.3	7.6	0.2	10	0.2	12.5	0.2	8.4	0.2	1.7	0.1
Magnetite	Fe_3O_4	P	1.9	0.2	2.5	0.1	2	0.1	2.8	0.1	6.6	0.2	10.3	0.2
Pseudobrookite	Fe_2TiO_5	P			0.3	0.1	0.3	0.1	0.3	0.1	0.1	0.1	0.5	0.1
Lime	CaO	P	0.1	0.1	0.1	0.1			0.1	0.1				
Protoenstatite	$Mg_2Si_2O_6$	P	1.2	0.2	1.2	0.1	0.7	0.2						
Naquite	FeSi	P	0.9	0.1	0.7	0.1	0.5	0.1	0.6	0.1	0.3	0.1		
Hematite	Fe_2O_3	I									2.1	0.1	1.9	0.1
Titanite	$CaTiSiO_5$	P									0.5	0.1		
Rutile	TiO_2	P			0.4	0.1	0.4	0.1	0.5	0.1			0.2	0.1
Quartz	SiO_2	N	0.1	0.04							8.9	0.1	13.3	0.1
Vaterite	$CaCO_3$	A	1	0.2	1.1	0.2	0.8	0.2	1	0.2	0.7	0.2		
Calcite	$CaCO_3$	A							0.3	0.1	4	0.1	17.9	0.2
Lepidocrocite	γ-FeO(OH)	A									2.8	0.9		
Corundum	Al_2O_3	M	3.3	0.2	2.9	0.2	1.7	0.2	3	0.2	5.6	0.2	0.8	0.2
Graphite	C	I	0.9	0.1	0.3	0.1	0.2	0.05						
Moissanite 2H	SiC	I											0.3	0.1
Albite	$NaAlSi_3O_8$	N											1.1	0.3
Clinoenstatite	$MgSiO_3$	I											2.1	0.3
Amorphous			3.5	2.2	2	1.7	6.8	1.5	3	1.7	12.1	1.8	31	0.9

Note: P-primary slag phase, A-Alteration product, N-natural contamination, M–milling contamination, I-industrial contamination. Stdev. = Standard deviation as calculated by Topas.

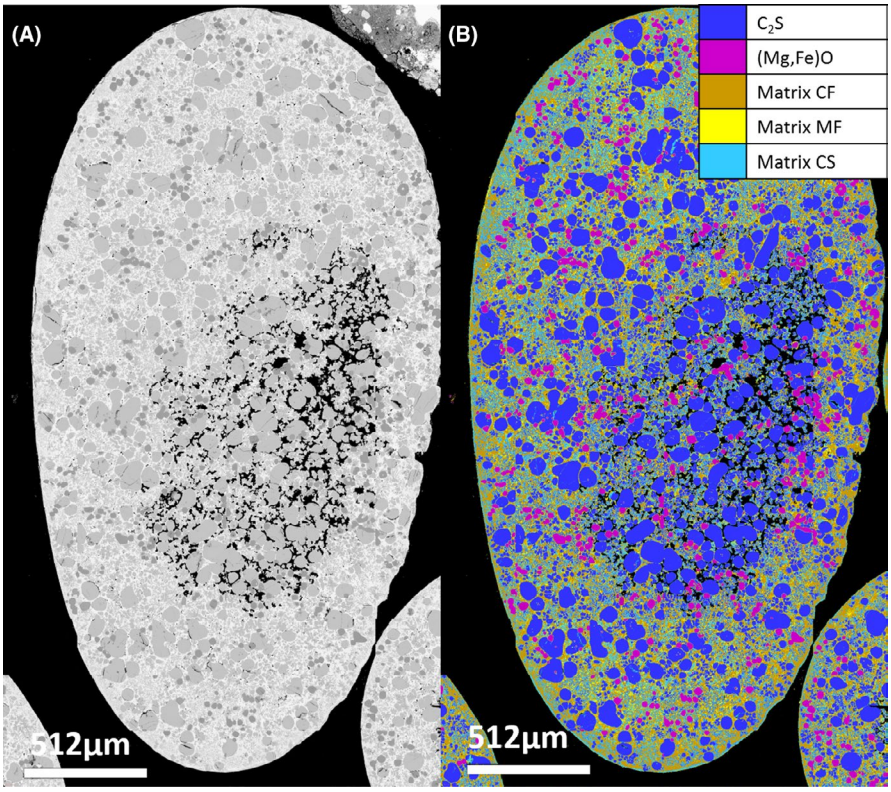

FIGURE A1 Air granulated converter slag 1-2 mm (A) SEM grayscale image (B) Phase map

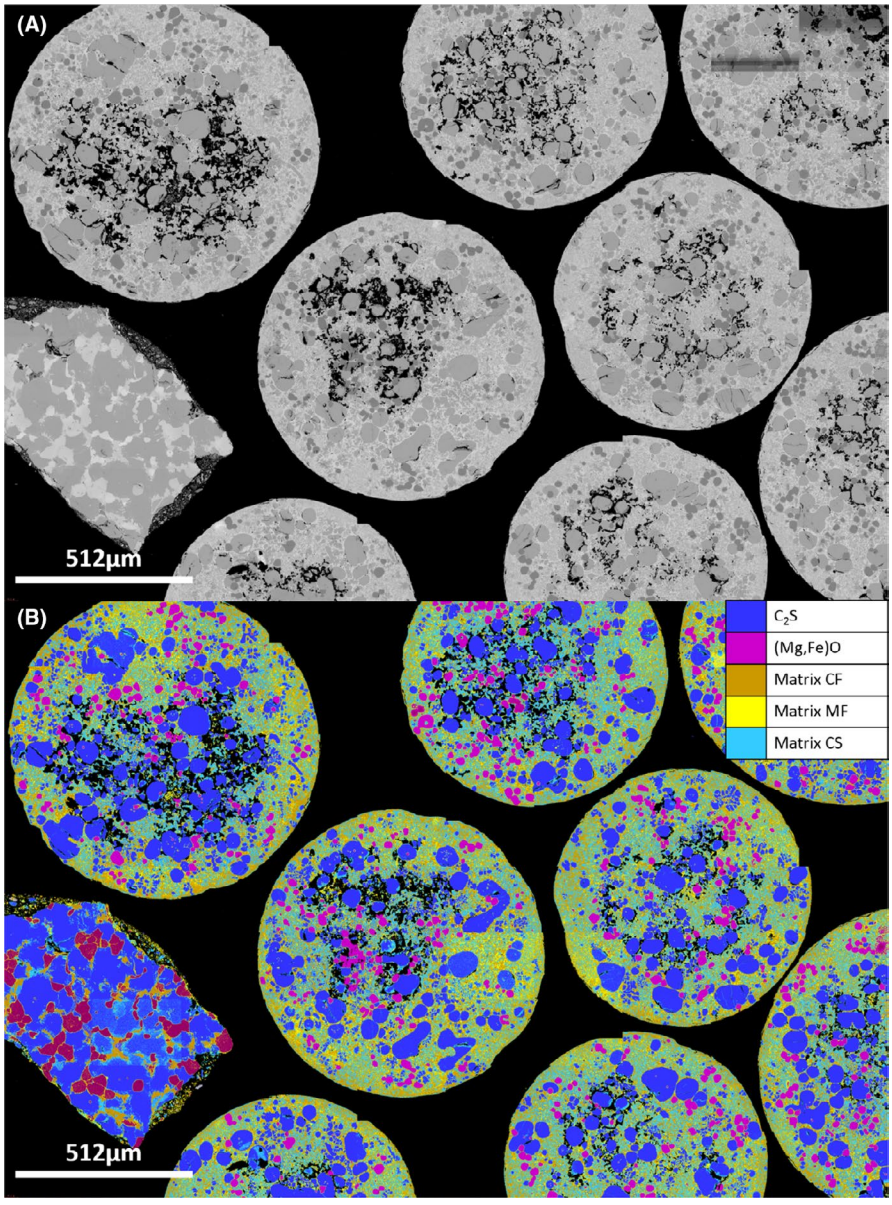

FIGURE A2 Air granulated converter slag 0.5-1 mm, lower right corner shows grain of industrially cooled converter slag (A) SEM grayscale image (B) Phase map